Irreducible Mass-Transport Limitations during a Heterogeneously Catalyzed Gas-Phase Chain Reaction: Oxidative Coupling of Methane

Pieter M. Couwenberg, Qi Chen,† and Guy B. Marin*

Laboratorium voor Chemische Technologie, Eindhoven University of Technology, P.O. Box 513, 5600 MB Eindhoven, The Netherlands

A heterogeneous reactor model was developed describing kinetic experiments on the heterogeneously catalyzed oxidative coupling of methane in a laboratory fixed-bed reactor. The catalyst produces radicals which react further through gas-phase reactions in the pores of the catalyst and in the interstitial phase. The reactor model accounts for the irreducible mass-transport limitations for the reactive radicals, which occur even at conditions where no mass-transport limitations occur for the molecules, both reactants and reaction products. The effects of these irreducible mass-transport limitations on the conversion and selectivity of the process were investigated and were found to be essential for an adequate description of experimental data.

Introduction

During the determination of intrinsic kinetics of a heterogeneous catalytic reaction, experiments have to be performed in such a way that internal and external concentration and temperature gradients can be neglected. Several criteria have been reported in the literature (Mears, 1971; Ergun, 1952; Weisz and Prater, 1954) which allow one to calculate the critical catalyst pellet sizes, temperature, pressure, and mass-flow rates. The criteria for mass-transport limitations usually concern limitations for the reactants and the products, because in most catalytic processes the reactants are converted through a series of steps involving only intermediates on the catalyst surface.

During some high-temperature processes, however, a different mechanism occurs: the catalyst produces reactive intermediates, e.g., radicals, which react further in the gas phase. An example of such a reaction is provided by the oxidative coupling of methane aimed at production of ethene. This process can be considered as a gas-phase chain reaction catalyzed by a solid (Lunsford, 1990; Baerns and Ross, 1992). Methane is converted on the catalyst surface to methyl radicals which either couple in the gas phase to form ethane or are oxidized to carbon oxides through a branched-chain reaction. Because methyl radicals are very reactive, transport limitations of these radicals are irreducible, i.e., the pellet size at which the internal concentration gradients would be negligible is much smaller than the minimal pellet size imposed by pressure drop considerations, in contrast to the classical transport limitations mentioned before.

The existence of irreducible transport limitations was reported before by Boudart (1968) for polymerization reactions, e.g., the gel effect, and for homogeneous radical reactions, e.g., the cage effect and the wall effect. In this paper it is shown that another type of irreducible mass-transport limitation exists, occurring during a heterogeneously catalyzed gas-phase chain reaction. Furthermore, the way to handle these irreducible transport phenomena mathematically during the determination of the reaction kinetics will be dealt with. Finally, the effects of these irreducible transport limitations on conversions and selectivities are investigated.

Typical Features of the Heterogeneously Catalyzed Oxidative Coupling of Methane

The kinetic model used during the simulations in this paper is discussed in detail by Couwenberg et al. (1995). Here only some typical features of this model, developed for a Sn/Li/MgO catalyst (Korf et al., 1989), will be given. The most important catalytic reaction during the oxidative coupling of methane is the production of methyl radicals (Ito et al., 1985; Aparicio et al., 1991; Reyes et al., 1993a; McCarty, 1992; Krylov, 1993) through the following catalytic cycle:

	σ_i
$O_2 + 2* \rightleftarrows 2O*$	1
$CH_4 + O* \rightarrow CH_3^{\cdot} + OH*$	4
$2OH* \rightleftarrows H_2O + O* + *$	2
$4CH_4 + O_2 \rightarrow 4CH_3^{\cdot} + 2H_2O$	

(1)

The catalytic radical production cycle provides a heterogeneous initiation which, at low pressures, is much faster than the homogeneous initiation. The produced methyl radicals react further in the gas phase where they can either couple to form ethane (2):

$$CH_3^{\bullet} + CH_3^{\bullet} + M \rightleftarrows C_2H_6 + M \qquad (2)$$

or react further through branched chains (Chen et al., 1991), of which a typical example is provided in Table 1.

Of course, such gas-phase reactions occur in the pores of the catalyst pellets as well as in the void space between the catalyst pellets, the so-called interstitial phase. In the branched chain (see Table 1), the methyl radical is oxidized to carbon monoxide with the simultaneous production of three hydroxy radicals. The branching reaction would thus lead to a high concentration of oxygen-containing radicals, resulting in low selectivities. However, it was found that the catalyst not only produces radicals but also quenches radicals (Tulenin et al., 1992; Sanches-Marcano et al., 1992). Couwenberg et al. (1995) showed that heterogeneous termination reaction (3) has to be included in the reaction mechanism to describe adequately the kinetic

* To whom correspondence should be addressed.

† Present address: KTI, P.O. Box 86, NL-2700 AB Zoetermeer, The Netherlands.

0888-5885/96/2635-0415$12.00/0 © 1996 American Chemical Society

Table 1. Typical Branched Chain and Rates of the Propagation Steps in the Center of the Void Space between the Catalyst Pellets (Conditions: see Table 2)

	σ_i	$r_{i,v}$/(mol m_g^{-3} s^{-1})
$CH_3^{\cdot} + HO_2^{\cdot} \rightarrow CH_3O^{\cdot} + OH^{\cdot}$	1	0.25
$CH_3O^{\cdot} + M \rightarrow CH_2O + H^{\cdot} + M$	1	0.25
$CH_2O + CH_3^{\cdot} \rightarrow CHO^{\cdot} + CH_4$	1	0.25
$CHO^{\cdot} + M \rightarrow CO + H^{\cdot} + M$	1	0.25
$O_2 + H^{\cdot} + M \rightarrow HO_2^{\cdot} + M$	2	0.35
$CH_4 + HO_2^{\cdot} \rightarrow CH_3^{\cdot} + H_2O_2$	1	0.05
$H_2O_2 \rightarrow 2OH^{\cdot}$	1	0.08
$CH_3^{\cdot} + 2O_2 \rightarrow CO + 3OH^{\cdot}$		

Table 2. Conditions of an Experiment Used for the Example Simulation

p_t/kPa	117
$CH_4/O_2\|_0$/(mol mol^{-1})	3.7
T/K	973
$W/F_{t,0}$/(kg s mol^{-1})	3.8
d_p/m	$2.5\ 10^{-4}$
X_{CH_4}/%	8.1
X_{O_2}/%	29.6

experiments over a tin-promoted lithium on magnesia catalyst:

$$4HO_2^{\bullet} \xrightarrow{\text{surface}} 2H_2O + 3O_2 \qquad (3)$$

This heterogeneous termination reaction lowers the concentration of oxygen-containing radicals and thus keeps the nonselective gas-phase reactions under control.

The Sn/Li/MgO catalyst also provides a route for the catalytic oxidation of methyl radicals via methoxy species toward carbon oxides and in particular to carbon dioxide:

$$CH_3^{\bullet} + O^* \rightarrow CH_3O^* \rightarrow \ldots \rightarrow CO_2 \qquad (4)$$

The branched chains, of which the one shown in Table 1 is the most important one, provide the major contribution to the formation of carbon oxides in the interstitial phase. Inside the catalyst pellets the catalytic oxidation dominates the production of carbon oxides.

Pellet-Scale Mass-Transport Limitations

The experimental reactor, used for the kinetic experiments, was designed such that no mass-transport limitations for the reactants or the reaction products occur. This was verified using the Weisz modulus (Weisz and Prater, 1954), which provides a useful criterion to verify whether intraparticle concentration gradients, due to diffusion limitations, can be neglected. At the conditions specified in Table 2 the Weisz modulus with respect to oxygen amounts to 0.003 at the reactor inlet, indicating that no significant concentration gradient develops for oxygen. External mass-transfer limitations can be neglected when the concentration difference between the bulk of the gas phase and the external surface results in a rate difference of less than 5%. The mass-transfer rate through a film surrounding a catalyst particle is proportional to the mass-transfer coefficient, the concentration difference, and the external surface area. Using the empirical correlation of Dwivedi and Upadhay (1977) to calculate the mass-transfer coefficient, this results in an oxygen concentration drop over the external film surrounding the catalyst particle of less than 0.1% of the bulk oxygen concentration. Since methane is available in excess and the rate of methane consumption is comparable to the rate of oxygen consumption, no gradients for methane will develop either.

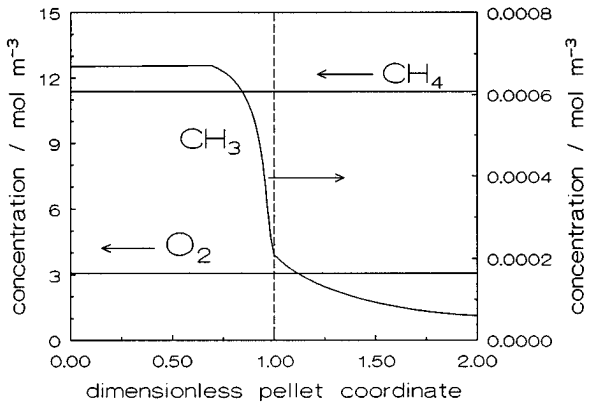

Figure 1. Calculated pellet-scale concentration profile of methyl radicals, methane, and oxygen. Conditions: see Table 2.

To assess whether mass-transport and mass-transfer limitations for the reactive intermediates can be neglected as well, the use of the Weisz modulus and mass-transfer coefficient is no longer straightforward. To calculate the Weisz modulus for a reactive intermediate, the concentration at the gas−solid interface and the net production rate inside the catalyst pellet must be known. The net production rate of a reactive intermediate equals the flux through the gas−solid interface. A mass-transfer coefficient cannot be applied anymore because mass transfer and reaction in the external film now occur simultaneously. Therefore, the continuity equations describing diffusion with simultaneous reaction in a pellet and the surrounding gas-phase must be integrated for each of the molecules and radicals involved (McCarty, 1992). Wolf (1994) performed a kinetic study for the heterogeneously catalyzed oxidative coupling of methane where external mass-transfer limitations had to be accounted for, by using a mass-transfer coefficient.

Figure 1 shows the solution of such a set of continuity equations for methyl radicals, methane, and oxygen. These results concern catalyst pellets with a diameter of 2.5×10^{-4} m at the conditions specified in Table 2. As was already predicted using the standard criteria, no significant concentration gradients develop for methane and oxygen. For methyl radicals, however, very steep relative internal and external concentration gradients exist, due to the very high reactivity of the surface-produced methyl radicals and, hence, the much lower absolute concentration level. All other radicals involved in the kinetic network develop significant concentration gradients on the pellet scale as well. The differential selectivity toward C_2 products at the axial position corresponding to Figure 1 amounts approximately to 55%. If these concentration gradients are not accounted for, the calculated differential selectivity amounts to 45%. This clearly shows that the strong internal and external concentration gradients must be accounted for during the kinetic modeling of the heterogeneously catalyzed oxidative coupling of methane.

Reactor Model Equations

In the previous paragraph it was shown that due to the high reactivity of the surface-produced radicals it is necessary to account for internal mass-transport

limitations and external mass-transfer limitations during the simulation of the experimental results obtained in the laboratory fixed-bed reactor. Hence, it is necessary to use a heterogeneous model, i.e., a model that explicitly distinguishes between a solid phase, i.e., the catalyst pellets, and a fluid phase, i.e., the gas phase in between the catalyst pellets (Froment and Bischoff, 1990). The solid phase and the fluid phase will be called the intraparticle phase and the interstitial phase in what follows.

Since the laboratory reactor was operated in the plug-flow regime (Cleland and Wilhelm, 1956) without radial temperature gradients (Mears, 1971), concentration gradients on the reactor scale only occur in the axial direction. Therefore, a one-dimensional heterogeneous model can be used.

The use of the commonly applied film model to describe mass transfer is not possible in the laboratory reactor since the film thickness is approximately equal to the pellet diameter at all investigated conditions. The film thickness follows from the ratio between the molecular diffusivity and the value of the mass-transfer coefficient. In the reactor model equations mass transfer from the interstitial phase to the gas−solid interface was therefore described by molecular diffusion with simultaneous gas-phase reactions. This approach to describe mass transfer to a pellet is very similar to the approach followed by Nelson and Galloway (1975) to calculate the values for mass-transfer coefficients at low Reynolds numbers in packed-bed reactors. Internal mass transport occurs simultaneously with catalytic reactions and gas-phase reactions in the pores of the catalyst pellet, which can be described by eq 6, which was also used to calculate the profiles shown in Figure 1. Although the Stefan−Maxwell theory is recommended to describe molecular diffusion in a multicomponent system (Wesselingh and Krishna, 1990), the use of Fick's law is permitted as in all experiments methane is present in large excess. The diffusion of all other components could, therefore, be considered as diffusion of this component in methane. Furthermore, the overall methane coupling reaction is approximately equimolar. The Stefan flow caused by the nonequimolar counterdiffusion and resulting in acceleration or retardation of mass transport can thus be neglected.

Because the laboratory reactor was heated by a fluidized sand bed oven, the measured axial temperature gradients were insignificantly small. Also the pressure drop over the reactor (Ergun, 1952) was low enough to be negligible. Therefore, only the continuity equations of all the components in the kinetic network had to be integrated. The volumetric flow rate through the reactor, F_v, was assumed to be constant. The above considerations led to the following model equations with corresponding boundary conditions:

Interstitial phase:

$$\frac{F_v}{\epsilon_b A_s}\frac{\partial C_{i,g}}{\partial z} = \frac{D_i}{r}\frac{\partial}{\partial r}\left(r\frac{\partial C_{i,g}}{\partial r}\right) + R_{i,g} \qquad (5)$$

Intraparticle phase:

$$-\frac{D_{e,i}}{\xi^2}\frac{\partial}{\partial \xi}\left(\xi^2\frac{\partial C_{i,c}}{\partial \xi}\right) = R_{i,c} + \epsilon_c R_{i,g} \qquad (6)$$

Boundary conditions:

$$z = 0 \wedge 0 < r < \frac{d_v}{2}: \quad C_{i,g} = C_{i,0} \qquad (7)$$

$$z > 0 \wedge r = 0: \quad \frac{\partial C_{i,g}}{\partial r} = 0 \qquad (8)$$

$$z > 0 \wedge r = \frac{d_v}{2}: \quad -a_g D_i \frac{\partial C_{i,g}}{\partial r} = a_c D_e \frac{\partial C_{i,c}}{\partial \xi} \qquad (9)$$

$$\xi = 0: \quad \frac{\partial C_{i,c}}{\partial \xi} = 0 \qquad (10)$$

$$\xi = \frac{d_p}{2}: \quad C_{i,c} = C_{i,g} \qquad (11)$$

The gas−solid interfacial surface area, a_g, and the external surface area of the catalyst, a_c, are not equal because the catalyst bed is diluted with an inert material to avoid radial temperature gradients. The balances for the surface components in the reaction network are not explicitly part of the reactor model. The concentrations of the latter were obtained directly from algebraic equations featuring only the concentrations of the gas-phase species, CH_4, O_2, CO_2, C_2H_4, and C_2H_6. These algebraic equations were derived using a Langmuir−Hinshelwood treatment and making the appropriate quasi-equilibrium and steady-state assumptions (Couwenberg, 1995).

The model's coordinate system is clarified in Figure 2. On the reactor scale only one coordinate, z going from 0 to L, exists as plug flow is assumed. Although one coordinate on the pellet scale would be sufficient to determine the position in the interstitial phase and intraparticle phase, it is convenient to distinguish between two coordinates: ξ being the coordinate of a point starting from the center of the pellet and r being the coordinate of a point starting from the center of the interstitial phase. The use of a spherical coordinate system for the intraparticle phase and a cylindrical coordinate system for the interstitial phase simplifies the solution procedure described later, since it allows one to use symmetrical polynomials as trial functions during orthogonal collocation (Finlayson, 1972), and, therefore, the boundary conditions at $\xi = 0$ and $r = 0$ are automatically fulfilled. To test the influence of the geometry of the interstitial phase, a reactor model with a spherical geometry of the interstitial phase was also applied. The calculated conversions and selectivities at the reactor outlet were, however, not significantly altered.

Determination of d_v. The physical meaning of d_v is the average distance between two catalyst pellets. The value of d_v follows from the relation between the total gas-phase volume and the interfacial surface area, a_g, in the reactor. It can be derived that the value of d_v is only dependent on the bed porosity and the catalyst pellet diameter according to the following relation:

$$\frac{d_v}{2} = \frac{d_p}{3}\left(\frac{\epsilon_b}{1-\epsilon_b}\right) \qquad (12)$$

Solution Procedure. The applied kinetic model contains 23 gas-phase components, i.e., 13 molecules and 10 radicals. As mentioned previously, the concentrations of the surface species follow directly from the

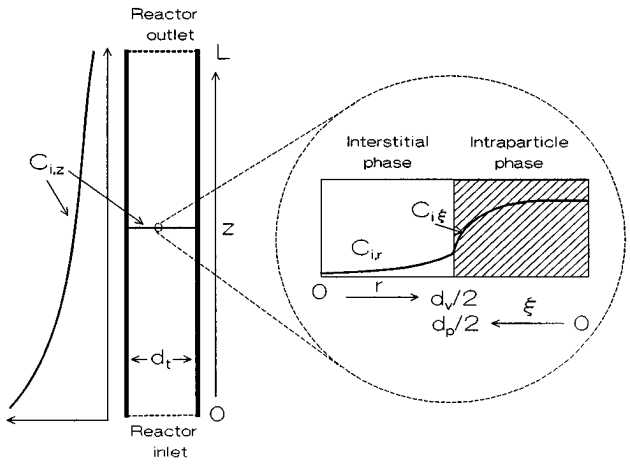

Figure 2. Schematical representation of the one-dimensional heterogeneous model accounting for mass-transport and mass-transfer limitations.

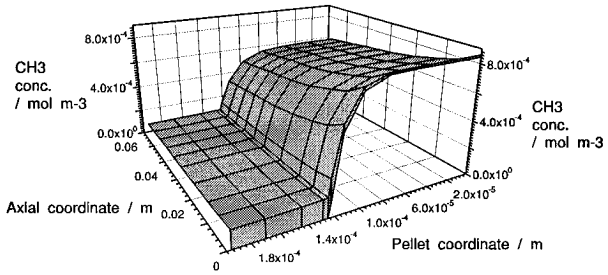

Figure 3. Calculated methyl-radical concentration profile on the pellet scale and reactor scale. Conditions: see Table 2.

concentration of gas-phase species through algebraic relations. The above reactor model equations, therefore, consist of a set of 23 stiff partial-differential equations (5) which are coupled with 23 ordinary differential equations (6) through their boundary conditions (7−11). These equations can be solved by discretization in the *r*- and ξ-direction using orthogonal collocation (Finlayson, 1972). This discretization results in a set of ordinary differential equations, with the axial reactor coordinate as the independent variable, coupled to algebraic equations, which was solved applying the method of Gear (1971).

Simulation Results

Simulation of an experiment in the laboratory reactor was performed using the above reactor model and the kinetic model described by Couwenberg et al. (1995). The conditions at which the simulation is performed are given in Table 2.

Among the 23 gas-phase species, six different types can be distinguished, namely, (1) reactants (CH_4 and O_2), (2) products (H_2, H_2O, CO, CO_2, C_2H_2, C_2H_4, C_2H_6, C_3H_6, and C_3H_8), (3) reactive molecules (H_2O_2 and CH_2O), (4) surface-produced reactive intermediates ($CH_3^{\cdot}$, $C_2H_5^{\cdot}$, and $C_2H_3^{\cdot}$), (5) surface-terminated reactive intermediates ($HO_2^{\cdot}$), and (6) gas-phase reactive intermediates ($H^{\cdot}$, $O^{\cdot}$, $OH^{\cdot}$, $CHO^{\cdot}$, $CH_3O^{\cdot}$, and $C_3H_7^{\cdot}$).

The characteristic concentration profiles of the surface-produced reactive intermediates, $CH_3^{\cdot}$, the surface-terminated reactive intermediates, $HO_2^{\cdot}$, and the gas-phase reactive intermediates, $H^{\cdot}$, are shown in Figures 3−5. The intraparticle and interstitial concentrations are plotted versus the axial reactor position and the pellet coordinate. The origin of the pellet-coordinate axis represents the center of the catalyst pellet, the

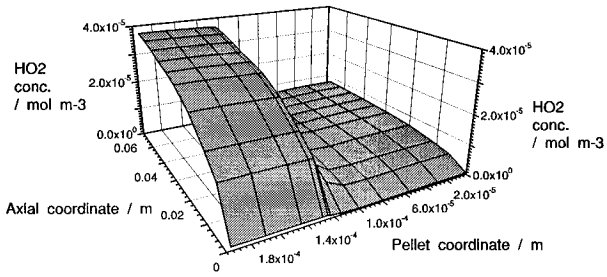

Figure 4. Calculated hydrogen−peroxy radical concentration profile on the pellet scale and reactor scale. Conditions: see Table 2.

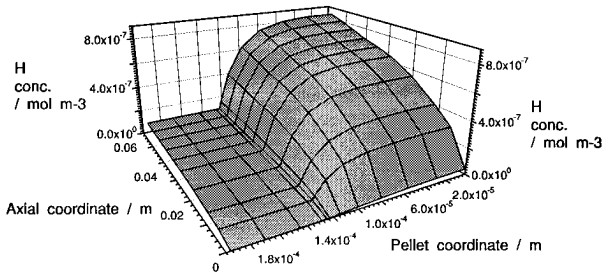

Figure 5. Calculated hydrogen-radical concentration profile on the pellet scale and reactor scale. Conditions: see Table 2.

external surface of the catalyst pellet is located at 1.25×10^{-4} m, and the space between 1.25×10^{-4} and 1.95×10^{-4} m corresponds to the interstitial gas phase. The development of pellet-scale concentration gradients for the reactive intermediates, as was shown in Figure 1, is confirmed by these figures. Again no significant pellet-scale concentration gradients were found for the reactants. The strong concentration gradients for the reactive intermediates are caused by their high consumption rates compared to their diffusion rates. The reactivity of a component can be quantified by the use of the lifetime of a radical (McCarty, 1992) defined as the reciprocal of the pseudo-first-order rate coefficient. The consumption and diffusion rates can be compared by the use of the diffusion length (McCarty, 1992).

$$\lambda_i = (D_i/k_1)^{1/2} \tag{13}$$

These two quantities can only be calculated after the solution of eqs 5−11 because the local concentration and consumption rate of each component must be known.

Table 3 shows the calculated concentration and corresponding consumption rate of six different types of components in the center of the catalyst pellet. The local consumption rate is the sum of the rates of the catalytic and gas-phase reactions. Furthermore, this table shows the pseudo-first-order rate coefficient, the lifetime of the components, the effective internal diffusion coefficient, and the diffusion length. Obviously, the diffusion lengths of the reactant, O_2, and the product, C_2H_6, are larger than the pellet diameter, indicating that the diffusion rate of these components is high enough to prevent the development of significant pellet-scale concentration gradients at conditions at the reactor outlet.

For methanal the diffusion length is somewhat shorter than the pellet diameter, resulting in a small pellet-scale concentration gradient. For the other three components the diffusion length is much smaller than the pellet diameter, and therefore a significant concentration gradient develops. In the center of the catalyst pellet the consumption rates of the reactive intermedi-

Table 3. Calculated Concentration, Consumption Rate, Pseudo-First-Order Rate Coefficient, Lifetime, Effective Diffusion Coefficient, and Diffusion Length

comp.	C^a/(mol m^{-3})	R_v/(mol m$_c^{-3}$ s^{-1})	k_1/s^{-1}	τ/s	D_e/(m$_g^3$ m$_c^{-1}$ s^{-1})	λ_i/m
O_2	2.1	27.2	46.3	0.02	8.0×10^{-6}	4.2×10^{-4}
C_2H_6	0.19	2.1	39.7	0.03	5.7×10^{-6}	3.7×10^{-4}
CH_2O	1.0×10^{-3}	0.5	1785	0.0005	6.9×10^{-6}	6.2×10^{-5}
$CH_3^{\cdot}$	5.9×10^{-4}	23.9	1.5×10^5	6.6×10^{-6}	$8.4\ 10^{-6}$	7.5×10^{-6}
$HO_2^{\cdot}$	8.0×10^{-6}	1.6	7.1×10^5	1.4×10^{-6}	1.4×10^{-5}	4.4×10^{-6}
$H^{\cdot}$	8.3×10^{-7}	2.1	9.1×10^6	1.1×10^{-7}	4.4×10^{-5}	2.2×10^{-6}

[a] Calculated at the reactor outlet in the center of the catalyst pellet. Conditions: see Table 2.

ates are equal to their production rates; i.e., their concentration follows from the balance between production and consumption. This explains the flat part in the intraparticle concentration profile of the methyl radicals; see Figure 3. At a distance from the external surface comparable to the diffusion length, the concentration of the methyl radical starts to decrease due to diffusion into the interstitial phase. In the interstitial phase the concentration of methyl radicals is much lower because of the much lower production rate of the methyl radicals. Along the axial coordinate the concentration of the methyl radicals decreases since the catalytic production rate decreases because of the lower methane and oxygen concentration, and the increasing concentration of carbon dioxide. Carbon dioxide is known to inhibit the reaction rate for Li/MgO-based catalysts due to carbonate formation (Korf et al., 1987; Wang et al., 1993).

The intraparticle concentration of the hydrogen−peroxy radical (see Figure 4) is much lower than the interstitial concentration, because the intraparticle consumption rate which is mainly determined by the heterogeneous termination (3) is much higher than the consumption rate in the interstitial phase. In the axial direction the interstitial hydrogen−peroxy concentration keeps increasing due to the increase in the ethane concentration. It was shown by Chen et al. (1994a) that increasing the ethane concentration leads to higher propagation rates in the branched-chain gas-phase reaction mechanism. This leads to increasing the total radical concentrations and, hence, to an increasing importance of the nonselective gas-phase reactions.

The intraparticle lifetime of the hydrogen radical, i.e., the lifetime calculated at the conditions in the center of the catalyst pellet (see Table 3), is so low that its concentration everywhere in the reactor is completely determined by the balance between production and consumption and thus by the local concentrations of all other species in the network (see Figure 5). The intraparticle concentration of the hydrogen radical is higher than the interstitial concentration because the total intraparticle radical concentration is higher as a result of the heterogeneous initiation reactions. Again the concentration increases along the axial coordinate due to an increasing ethane concentration.

Effects on Selectivity

The effects of the irreducible diffusion limitations of the reactive intermediates on the selectivity were investigated by changing the pellet diameters. The effect of pellet diameter on selectivity was also investigated by Follmer et al. (1989), Schiebisch et al. (1991), and Reyes et al. (1993b). Follmer et al. (1989) experimentally found an increase in the selectivity with increasing pellet diameter and attributed this to the lower intraparticle concentration of oxygen. A low oxygen concentration can improve the C_2 selectivity. Reyes et al. (1993b) calculated a decrease in selectivity with increasing pellet sizes at an inlet methane-to-oxygen ratio of 2.0 and only a very small selectivity increase at an inlet methane-to-oxygen ratio of 20.0. The decrease in selectivity at low inlet methane-to-oxygen ratio was attributed to the occurrence of transport limitations of the C_2 molecules, resulting in a rising contribution of their secondary reactions toward CO_x products. At low pellet diameters where no transport limitations occur for the reactants and the products, no effects of the pellet diameter on the selectivity were reported. Scheibisch et al. (1991) measured a decreasing selectivity with increasing pellet diameter and related this observation to diffusion limitations of the C_2 components.

The present study focuses on the effects of the transport limitations of the reactive intermediates. Therefore, all calculations were performed at conditions where no transport limitations occur for the reactants and the products, thus excluding the beneficial effects of the low intraparticle oxygen concentration and the negative effect of the increasing contribution of the secondary oxidation of C_2 products.

On the basis of the calculated concentration profile of the methyl radical, an increase in selectivity is expected with increasing pellet diameter, since the volume where the high methyl-radical concentration exists is larger when larger pellets are applied. This would favor their coupling toward ethane, since this is a second-order reaction, all other steps being first order with respect to the methyl-radical concentration. The results of the calculations presented in Figure 6, however, show a decrease in the C_{2+} selectivity with increasing pellet sizes. This is caused by the decrease in the ratio of the external surface area and the volume of the interstitial phase, resulting in a lower contribution of the heterogeneous termination reaction on the total termination of the gas-phase chain reactions in the interstitial phase. This results in a higher concentration of the hydrogen−peroxy radical concentration in the interstitial phase. Table 4 indeed clearly shows that the $HO_2^{\cdot}$ concentration in the center of the interstitial phase increases with increasing pellet diameter. The higher interstitial $HO_2^{\cdot}$ concentration results in a higher rate of the nonselective gas-phase reactions in the interstitial phase and thus in lower selectivities. This was verified by removing the heterogeneous termination from the kinetic network. The calculated selectivity versus pellet diameter plots without this reaction are also shown in Figure 6. It can be seen that the selectivity indeed increases with increasing pellet size. Another significant effect of neglecting the heterogeneous termination is the much lower selectivity. This is caused by the higher $HO_2^{\cdot}$ concentration in the case that no heterogeneous termination is considered, as is shown in Table 4. This table also shows that the

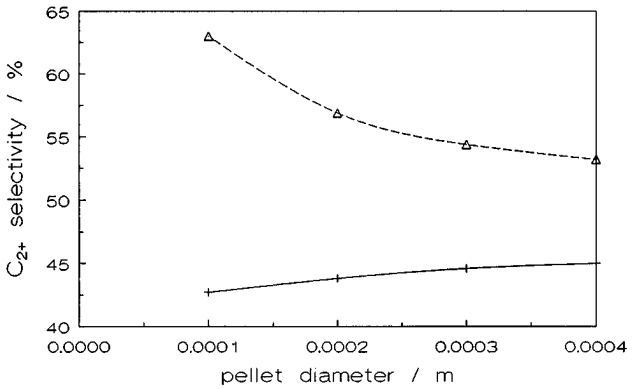

Figure 6. Selectivity vs d_p calculated with the kinetic model of Couwenberg et al. (1995) with (- - -) and without (—) a heterogeneous termination reaction. Conditions: see Table 2.

Table 4. Calculated $HO_2^{\cdot}$ Concentration in the Center of the Interstitial Phase with and without a Heterogeneous Termination (Conditions: see Table 2)

d_p/m	$C_{HO_2^{\cdot}}{}^a$/(mol m_g^{-3})	$C_{HO_2^{\cdot}}{}^b$/(mol m_g^{-3})
1.0×10^{-4}	2.5×10^{-5}	1.76×10^{-4}
2.0×10^{-4}	3.3×10^{-5}	1.75×10^{-4}
2.5×10^{-4}	3.7×10^{-5}	1.73×10^{-4}
3.0×10^{-4}	4.0×10^{-5}	1.72×10^{-4}
4.0×10^{-4}	4.7×10^{-5}	1.68×10^{-4}

[a] Calculated with a heterogeneous termination. [b] Calculated without a heterogeneous termination.

concentration of $HO_2^{\cdot}$ is almost independent of the pellet diameter, when no heterogeneous termination is considered.

The calculated methane conversion, corresponding to the calculations with the heterogeneous termination shown in Figure 6, is approximately constant at 8.0% with increasing pellet diameter, because no significant pellet-scale concentration gradients exist for the molecules involved in the kinetic network. It is shown by Couwenberg et al. (1995) that the consumption rate of methane is mainly determined by the catalytic reactions and thus only by the concentration of the species determining the rates of the catalytic reactions, i.e., CH_4, C_2H_4, C_2H_6, O_2, and CO_2.

Conclusions

Pellet-scale concentration gradients for the reactive intermediates in the heterogeneously catalyzed oxidative coupling of methane, e.g., methyl and hydrogen–peroxy radicals, can develop even at conditions where no significant concentration gradients exist for the reactants and the products. These concentration gradients are caused by the very high consumption rate of these intermediates compared to their transport rate by diffusion. During the kinetic modeling of the oxidative coupling of methane, these gradients should be considered, because the reactive intermediates play a key role in the reaction mechanism. Therefore, a heterogeneous reactor model explicitly accounting for mass-transport and mass-transfer limitations has to be applied.

An increase in selectivity with increasing pellet diameter is expected because the high intraparticle methyl-radical concentration favors their coupling, since this is the only second-order reaction with respect to the methyl radicals. The complex interplay between the catalytic reactions and the reactions in the gas phase and the role of mass-transport herein, however, makes an a-priori prediction of the effects of diffusion limitations difficult. Calculations showed a decrease in selectivity with increasing pellet diameter. This could be explained by the decreasing importance of the heterogeneous termination on the gas-phase reactions in the interstitial phase, due to a decreasing ratio between the gas–solid interfacial surface area and the interstitial volume. The resulting higher $HO_2^{\cdot}$ concentration causes a decrease in the selectivity because the nonselective gas-phase reactions gain importance.

Acknowledgment

The financial support provided by the commission of the European Communities in the framework of the JOULE programme, subprogramme Energy from Fossil Sources, Hydrocarbons, No. JOUF-0044-C, is gratefully acknowledged.

Notation

Roman Symbols

A_s = reactor cross-sectional surface area, m_r^2
a_c = total external catalyst surface area, $m_c^2\ m_r^{-3}$
a_g = gas–solid interfacial surface area, $m_i^2\ m_r^{-3}$
$C_{i,c}$ = concentration of component i in the intraparticle phase, mol m_g^{-3}
$C_{i,g}$ = concentration of component i in the interstitial phase, mol m_g^{-3}
D_i = molecular diffusion coefficient, $m_g^3\ m_g^{-1}\ s^{-1}$
$D_{e,i}$ = effective internal diffusion coefficient, $m_g^3\ m_c^{-1}\ s^{-1}$
d_v = avarage distance between two catalyst pellets, m
d_p = pellet diameter, m
F_v = volumetric flow rate, $m_g^3\ s^{-1}$
k_1 = pseudo-first-order rate coefficient, s^{-1}
L = reactor length, m
p_t = pressure, kPa
r = radial coordinate, m
$R_{i,g}$ = net production rate of component i through gas-phase reactions, mol $m_g^{-3}\ s^{-1}$
$R_{i,c}$ = net production rate of component i through catalytic reactions, mol $m_c^{-3}\ s^{-1}$
T = temperature, K
W = catalyst mass, kg
X = conversion, %
z = axial coordinate, m

Greek Symbols

ϵ_b = bed porosity, $m_g^3\ m_r^{-3}$
ϵ_c = catalyst porosity, $m_g^3\ m_c^{-3}$
λ_i = diffusion length of component i, m
ξ = pellet coordinate, m
τ = lifetime, s

Literature Cited

Aparicio, L. M.; Rossini, S. A.; Sanfilippo, D. G.; Rekoske, J. A.; Treviño, A. A.; Dumesic, J. A Microkinetic Analysis of Methane Dimerization Reaction. *Ind. Eng. Chem. Res.* **1991**, *30*, 2114.

Baerns, M.; Ross, J. H. R. Catalytic Chemistry of Methane Conversion. In *Perspectives in Catalysis*; Thomas, J. M., Zamaraev, K. I., Eds.; IUPAC Monograph; Blackwell Scientific Publications: Oxford, U.K., 1992.

Boudart, M. *Kinetics of Chemical Processes*, 1st ed.; Prentice-Hall: Englewood Cliffs, NJ, 1968.

Chen, Q.; Hoebink, J. H. B. J.; Marin, G. B. Kinetics of the Oxidative Coupling of Methane at Atmospheric Pressure in the Absence of Catalyst. *Ind. Eng. Chem. Res.* **1991,** *30*, 2088.

Chen, Q.; Couwenberg, P. M.; Marin, G. B. The Oxidative Coupling of Methane with Cofeeding of Ethane. *Catal. Today* **1994a**, *21*, 309.

Chen, Q.; Couwenberg, P. M.; Marin, G. B. Effect of Pressure on the Oxidative Coupling of Methane in the Absence of Catalyst. *AIChE J.* **1994b**, *40* (3), 521.

Cleland, F. A.; Wilhelm, R. H. Diffusion and Reaction in Viscous Flow Tubular Reactor. *A.I.Ch.E. J.* **1956**, *2* (4), 489.

Couwenberg, P. M. Gas-Phase Chain Reactions Catalyzed by Solids: The Oxidative Coupling of Methane. Ph.D. Thesis, Eindhoven University of Technology, Eindhoven, The Netherlands, 1995.

Couwenberg, P. M.; Chen, Q.; Marin, G. B. Kinetics of a Gas-Phase Chain Reaction Catalysed by a Solid: The Oxidative Coupling of Methane. Submitted to *Ind. Eng. Chem. Res.* 1995.

Dwivedi, P. N.; Upadhyay, S. N. Particle-Fluid Mass Transfer in Fixed and Fluidized Beds. *Ind. Eng. Chem. Process Des. Dev.* **1977**, *16* (2), 157.

Ergun, S. Fluid Flow through Packed Columns. *Chem. Eng. Prog.* **1952**, *48* (2), 89.

Finlayson, B. A. The Method of Weighted Residuals an Variational Principles, with Application in Fluid Mechanics, Heat and Mass Transfer. In *Mathematics in Science and Engineering*; Bellman, R., Ed.; Academic Press: New York, 1972; Vol. 87.

Follmer, G.; Lehmann, L.; Baerns, M. Effect of Transport Limitations on C_{2+} Selectivity in the Oxidative Coupling Reaction using a NaOH/CaO Catalyst. *Catal. Today* **1989**, *4* (4), 323.

Froment, G. F.; Bischoff, K. B. *Chemical Reactor Analysis and Design*, 2nd ed.; John Wiley and Sons: New York, 1990.

Gear, C. W. The Automatic Integration of Ordinary Differential Equations. *Commun. ACM* **1971,** *14*, 176.

Ito, T.; Wang, J.-X.; Lin, C. H.; Lunsford, J. H. Oxidative dimerization of methane over a lithium-promoted magnesium oxide catalyst. *J. Am. Chem. Soc.* **1985**, *107*, 5062.

Korf, S. J.; Roos, J. A.; de Bruijn, N. A.; van Ommen, J. G.; Ross, J. R. H. Influence of CO_2 on the Oxidative Coupling of Methane over a Lithium Promoted Magnesium Oxide Catalyst. *J. Chem. Soc., Chem. Commun.* **1987,** 1433.

Korf, S. J.; Roos, J. A.; Veltman, L. J.; van Ommen, J. G.; Ross, J. R. H. Effect of additives on Lithium doped Magnesium Oxide Catalysts Used in the Oxidative Coupling of Methane. *Appl. Catal.* **1989,** *56*, 119.

Krylov, O. V. Catalysts for Methane Oxidative Coupling and its Reaction Mechanism. *Kinet. Catal.* **1993,** *34* (1), 11.

Lunsford, J. H. The Catalytic Conversion of Methane to Higher Hydrocarbons. *Catal. Today* **1990,** *6*, 235.

McCarty, J. G. Mechanism of Cooxidative Methane Dimerization Catalysis: Kinetic and Thermodynamic Aspects. In *Methane Conversion by Oxidative Processes*; Wolf, E. E., Ed.; Van Nostrand Reinhold: New York, 1992.

Mears, D. E. Diagnostic Criteria for Heat Transport Limitations in Fixed Bed Reactors. *J. Catal.* **1971,** *20*, 127.

Nelson, P. A.; Galloway, T. R. Particle-to-Fluid Heat and Mass Transfer in Dense Systems of Fine Particles. *Chem. Eng. Sci.* **1975**, *30*, 1.

Reyes, S. C.; Kelkar, C. P.; Iglesia, E. Kinetic-transport Models and the Design of Catalysts for the Oxidative Coupling of Methane. *Catal. Lett.* **1993a,** *19*, 167.

Reyes, S. C.; Iglesia, E.; Kelkar, C. P. Kinetic-Transport Models of Bimodal Reaction Sequences—I. Homogeneous and Heterogeneous Pathways in Oxidative Coupling of Methane. *Chem. Eng. Sci.* **1993b**, *48* (14), 2643.

Sanches-Marcano, J.; Mirodatos, C.; Wolf, E. E.; Martin, G. A. Inhibition of the Gas Phase Oxidation of Ethylene by Various Solids and Influence of their Addition on the Catalytic Properties of Lanthanum Oxide towards the Oxidative Coupling of Methane. *Catal. Today* **1992**, *13*, 227.

Schiebisch, J.; Bartsch, S.; Dittmeyer, R.; Hofmann, H. Stoftransporteffekte bei der Oxidativen Kopplung von Methan. *Chem.-Ing.-Tech.* **1991,** *4*, 359.

Tulenin, Yu.P.; Kadushin, A. A.; Seleznev, V. A.; Shestakov, A. F.; Korchak, V. N. Effect of Pressure on the Process of Methane Oxidative Dimerization. Part 1. The Mechanism of Heterogeneous Inhibition of the Gas Phase Reactions. *Catal. Today* **1992**, *13*, 329.

Wang, D.; Xu, M.; Shi, C.; Lunsford, J. H. Effect of Carbon Dioxide on the Selectivities Obtained During the Partial Oxidation of Methane and Ethane over Li^+/MgO Catalysts. *Catal. Lett.* **1993**, *18*, 323.

Weisz, P. B.; Prater, C. D. Interpretation of Measurements in Experimental Catalysis. *Adv. Catal.* **1954,** *6*, 143.

Wesselingh, J. A.; Krishna, R. *Mass Transfer*; Ellis Horwood: London, 1990.

Wolf, D.; Microkinetic Analysis of the Oxidative Coupling of Methane. Dependency of Rate Constants on the Electrical Properties of $(CaO)_x(CeO_2)_{1-x}$ catalyst. *Catal. Lett.* **1994,** *27* (1−2), 207.

Received for review May 10, 1995
Revised manuscript received November 6, 1995
Accepted November 16, 1995[⊗]

IE9502852

[⊗] Abstract published in *Advance ACS Abstracts*, January 15, 1996.